Journal of Materials Chemistry A

Enhancing exciton diffusion by reducing energy disorder in organic solar cells

Journal:	*Journal of Materials Chemistry A*
Manuscript ID	TA-ART-09-2022-007113.R1
Article Type:	Paper
Date Submitted by the Author:	17-Oct-2022
Complete List of Authors:	Xue, Peiyao; Peking University, School of Materials Science and Engineering Calascibetta, Adiel; State University of Milano-Bicocca, Department of Materials Science Chen, Kai; Victoria University of Wellington, School of Chemical and Physical Sciences Thorn, Karen; Victoria University of Wellington, School of Chemical and Physical Sciences Jiang, Yiting; Peking University Shi, Jiangjian; Institute of Physics, Chinese Academy of Sciences Jia, Boyu; Peking University Li, Mengyang; Donghua University, State Key Laboratory for Modification of Chemical Fibers and Polymer Materials Xin, Jingming; State Key Laboratory for Mechanical Behavior of Materials, Xi'an Jiaotong University Cai, Guilong; Chinese University of Hong Kong, Department of Physics Yang, Rui; Beijing University of Chemical Technology Lu, Heng; Peking University, School of Materials Science and Engineering Mattiello, Sara; State University of Milano-Bicocca, Materials Science Liu, Yao; Beijing University of Chemical Technology, material science and engineering ; Beijing Advanced Innovation Center for Soft Matter Science and Engineering Tang, Zheng; Center for Advanced Low-dimension Materials, Donghua University, Lu, Xinhui; The Chinese University of Hong Kong, Physics Ma, Wei; Xi'an Jiaotong University, State Key Laboratory for Mechanical Behavior of Materials Meng, Qingbo; Institute of Physics Chinese Academy of Sciences Hodgkiss, Justin; Victoria University of Wellington, School of Chemical and Physical Sciences Beverina, Luca; State University of Milano-Bicocca, Materials Science Han, Ray; Peking University, Materials Science and Engineering Zhan, Xiaowei; Peking University, Department of Materials Science and Engineering, College of Engineering

Enhancing exciton diffusion by reducing energy disorder in organic solar cells†

Peiyao Xue,[a] Adiel M. Calascibetta,[c] Kai Chen,[d] Karen E. Thorn,[d] Yiting Jiang,[a] Jiangjian Shi,[e] Boyu Jia,[a] Mengyang Li,[f] Jingming Xin,[g] Guilong Cai,[h] Rui Yang,[i] Heng Lu,[a] Sara Mattiello,[c] Yao Liu,[i] Zheng Tang,[f] Wei Ma,[g] Xinhui Lu,[h] Qingbo Meng,[e] Justin M. Hodgkiss,[d] Luca Beverina,[c] Ray P. S. Han,[j] and Xiaowei Zhan[a,b,*]

[a]School of Materials Science and Engineering, Peking University, Beijing 100871, China. *E-mail address*: xwzhan@pku.edu.cn

[b]Key Laboratory of Eco-functional Polymer Materials of Ministry of Education College of Chemistry and Chemical Engineering, Northwest Normal University, Lanzhou 730070, China

[c]Department of Materials Science, State University of Milano-Bicocca, Via Cozzi 55, Milano, Italy

[d]MacDiarmid Institute for Advanced Materials and Nanotechnology, School of Chemical and Physical Sciences, Victoria University of Wellington, Wellington 6010, New Zealand

[e]CAS Key Laboratory for Renewable Energy, Beijing Key Laboratory for New Energy Materials and Devices, Institute of Physics, Chinese Academy of Sciences, Beijing 100190, China

[f]Center for Advanced Low-Dimension Materials, State Key Laboratory for Modification of Chemical Fibers and Polymer Materials, College of Materials Science and Engineering, Donghua University, Shanghai 201620, China

[g]State Key Laboratory for Mechanical Behavior of Materials, Xi'an Jiaotong University, Xi'an 710049, China

[h]Department of Physics, The Chinese University of Hong Kong, New Territories 999077, Hong Kong, China

[i]Beijing Advanced Innovation Center for Soft Matter Science and Engineering, State Key Laboratory of Chemical Resource Engineering, Beijing University of Chemical Technology, Beijing 100029, China

[j]Jiangzhong Cancer Research Center, Jiangxi University of Chinese Medicine, Nanchang 330004, China.

†Electronic supplementary information (ESI) available. See DOI: 10.1039/x0xx00000x

Abstract: A highly crystalline, highly emissive, and wide-bandgap polymer AC174 with an extremely small Stokes shift is designed and synthesized in water, and is used to reduce system energetic disorder and increase exciton diffusion length of the classical PM6:Y6 blend system. AC174 is incompatible with PM6 and Y6, improves molecular packing, and reduces system energetic disorder. The long-range Förster resonance energy transfer between donor and acceptor is enhanced, and the exciton diffusion constant and exciton lifetime are increased, leading to longer exciton diffusion length and more efficient exciton dissociation and charge generation. The addition of AC174 simultaneously improves open-circuit voltage, short-circuit current density (J_{SC}) and fill factor of PM6:Y6 devices; especially the highest internal quantum efficiency approaches 100%, and the highest J_{SC} is 28.4 mA cm^{-2}. Ternary devices with 5% AC174 in donors achieve a power conversion efficiency of 17.2%, higher than those of the parent binary devices based on PM6:Y6 (15.9%) and AC174:Y6 (3.24%).

Introduction

Organic solar cells (OSCs) are regarded as a next-generation photovoltaic technology since they own some merits such as facile fabrication, light weight, flexibility, ecofriendliness and short energy payback time.[1,2] Fused-ring electron acceptors (FREAs) pioneered by the Zhan group show strong light absorption in visible and near-infrared (NIR) region, high electron mobility, low energy loss and stable film morphology,[3-9] and have been widely used in high-performance OSCs.[10-14] Thanks to the invention of FREAs, the maximum power conversion efficiencies (PCEs) of OSCs have exceeded 20%.[15]

Organic semiconductors usually have low dielectric constants (*ca.* 2-4) and strong phonon-electron coupling, and therefore light absorption of the photoactive layers generates strongly bound electron-hole pairs (excitons) with high binding energy (*ca.* 0.1-1 eV) instead of free charges.[16] Then, excitons diffuse to donor/acceptor (D/A) heterojunction interfaces and dissociate into free charges driven by energy offset between D/A.[17,18] Because excitons created in organic semiconductors generally have short lifetime and limited diffusion lengths (*ca.* 10-20 nm), intimately intermixing of donor and acceptor for generating more D/A interfacial contacts is necessary for efficient exciton dissociation,[19] yet leads to unfavourable charge transport and recombination. The trade-off between exciton dissociation and charge transport in OSC requires complex morphology optimization of the photoactive layers.[20-23] Thus, increasing exciton diffusion length is essential for improving device performance.

The exciton diffusion length, L_D, is given as $\sqrt{D\tau}$, where D is the exciton diffusion constant, and τ is the exciton lifetime.[24,25] The lifetime of singlet excitons is determined by

radiative and non-radiative decay processes and can be expressed as $\tau = 1/(k_R + k_{NR})$, where k_R is the rate of radiative decay and k_{NR} is the rate of non-radiative decay. According to the energy gap law, k_{NR} correlates with the energy gap between singlet ground state (S_0) and the lowest-energy singlet excited state (S_1); narrower energy gap leads to higher k_{NR} and shorter exciton lifetime.[26-28] In high-efficiency OSCs, narrow-bandgap (E_g) semiconductor materials (E_g < 1.5 eV)[29] are commonly used to improve the light absorption in NIR region. Accordingly, it is challenging to decrease the non-radiative decay and increase exciton diffusion length of narrow-bandgap photovoltaic materials.

To solve this problem, understanding the exciton transport mechanism is critical. The dominating exciton transport mechanism in OSCs is Förster resonance energy transfer (FRET), where FRET radius correlates with system energetic disorder.[30,31] In FRET model, excitons predominantly hop between aligned chromophores as they diffuse. If the energy disorder increases, the fraction of chromophores that are energetically available for energy transfer will decrease, leading to smaller FRET radius. The reduced FRET caused by the high systematic energetic disorder limits the exciton diffusion constant. Moreover, higher energy disorder leads to increased non-radiative relaxation,[32-35] which reduces the exciton lifetime according to the energy gap law. Decrease in exciton diffusion constant and exciton lifetime leads to short exciton diffusion length. Therefore, reducing system energetic disorder is the key to promote the FRET and minimize non-radiative decay, and finally increase exciton diffusion length in OSC devices.

In this work, we designed and synthesized a highly-crystalline wide-bandgap polymer donor, AC174 (Fig. 1a), and used it to reduce energetic disorder and enhance exciton diffusion in the representative PM6:Y6-based OSCs. AC174 is incompatible with PM6 and Y6, and tends to form an individual phase in the PM6:AC174:Y6 ternary blend. Adding a small amount of AC174 can not only maintain good D/A phase separation, which is beneficial for charge transport, but also improve PM6/Y6 molecular packing and decrease system energetic disorder. Due to the reduced energetic disorder, the exciton diffusion ability and exciton lifetime increase, leading to enhanced exciton diffusion length and exciton dissociation. As a result, the ternary OSCs based on PM6:AC174:Y6 exhibit a higher PCE value of 17.2% compared with the PM6:Y6 devices (15.9%), and achieve a greatly increased short-circuit current density (J_{SC}) over 28 mA cm^{-2}, which is among the highest J_{SC} values in OSC devices.

Results and discussion

Materials synthesis and characterization

AC174 was synthesized through Suzuki-Miyaura micellar cross-coupling in water. This particular protocol enables a large reduction in the amount of organic wastes generated by the manufacturing of organic semiconductors.[36] Detailed synthesis procedure is described in ESI and nuclear magnetic resonance spectrum of AC174 is shown in Fig. S1 (ESI†). Firstly, we investigated the basic properties of AC174. AC174 exhibits an intense π-π stacking in the out-of-plane direction (q_z = 1.45 Å^{-1}, d = 4.32 Å) with a face-on molecular orientation,

indicating AC174 is highly crystalline, as measured by grazing incidence wide-angle X-ray scattering (GIWAXS) method (Fig. 1b). AC174 in diluted dichloromethane solution shows an intense absorption ranging from 300 to 550 nm with an absorption peak at 488 nm; its solid film exhibits an absorption peak at 554 nm, and optical bandgap (E_g) is calculated to be 2.10 eV (Fig. S2, ESI†). AC174 solid film shows a strong fluorescence peaked at 589 nm. A quite small Stokes shift of 35 nm is observed, indicating a rigid backbone and a low reorganization energy of AC174, which facilitates to reduce energetic disorder and enhance charge transport according to the Marcus theory.[37] The highest occupied molecular orbital (HOMO) and the lowest unoccupied molecular orbital (LUMO) energy levels of AC174 are calculated to be –5.47 eV and –3.37 eV, respectively, according to the ultraviolet photoelectron spectrometer (UPS) spectra and UV-vis absorption spectra (Fig. S3, ESI†).

Then, we investigated optoelectronic properties of the PM6:AC174:Y6 blend (Fig. S4, ESI†). AC174, PM6 and Y6 thin films exhibit strong absorption in the regions of 400-600 nm, 500-700 nm and 600-900 nm, respectively (Fig. 1c), which are complementary yielding panchromatic absorption. The emission range of AC174 (550-700 nm) is heavily overlapped with the absorption range of PM6 (500-700 nm), which is beneficial for the FRET between AC174 and PM6. The energy level diagram of PM6, AC174 and Y6 is shown in Fig. 1d, where the HOMO energy levels of PM6 and AC174 were both measured by UPS method (Fig. S3, ESI†), and that of Y6 was adopted from the reference, also measured by the same method on the same equipment.[38] The HOMO energy level of AC174 is deeper than that of PM6, which may increase open-circuit voltage (V_{OC}) in ternary device.

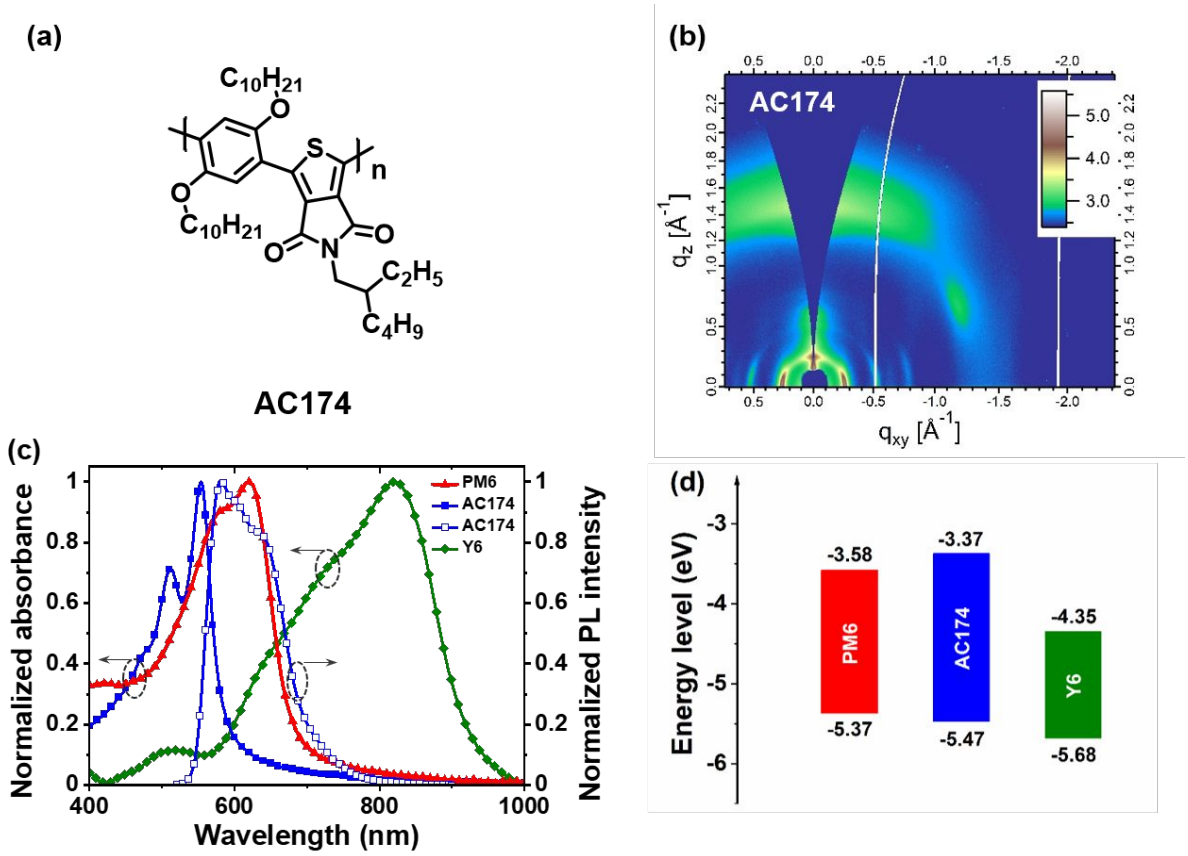

Fig. 1 (a) Chemical structure of AC174. (b) GIWAXS pattern of pure AC174 film. (c) normalized absorption spectra of PM6, AC174 and Y6 films and emission spectrum of AC174 film. (d) energy level diagram of PM6, AC174 and Y6.

Device performance and device physics

In order to study influence of AC174 on the performance of ternary OSCs, we adopted a conventional sandwich device structure of ITO glass/PEDOT:PSS/active layer/PNDIT-F3N/Ag to fabricate devices based on PM6:Y6 and PM6:AC174:Y6, respectively. Fig. 2a shows representative current density-voltage (*J*-*V*) curves of optimized PM6:Y6 and PM6:AC174:Y6 based OSCs measured under the illumination of an AM 1.5G solar simulator, 100 mW cm^{-2}. The PM6:Y6 device affords a V_{OC} of 0.812 V, J_{SC} of 26.6 mA

cm^{-2}, fill factor (FF) of 73.5%, and PCE of 15.9%. After adding a small amount of AC174, where the content of AC174 in donors (PM6 + AC174) is 5%, the optimized PM6:AC174:Y6 device achieves simultaneous improvement in V_{OC}, J_{SC} and FF, with a V_{OC} of 0.817 V, J_{SC} of 28.4 mA cm^{-2}, FF of 74.1%, leading to a greatly improved PCE of 17.2% (Table 1). The device performance data with different AC174 contents are listed in Table S1 (ESI†), and corresponding *J-V* curves and external quantum efficiency (EQE) spectra are shown in Fig. S5 (ESI†). As the weight ratio of AC174 in donors increases, V_{OC} shows small changes, while J_{SC} and FF show the tendency of increasing first and decreasing then (Fig. S6, ESI†). Interestingly, when the content of AC174 in the donors reaches 50%, the PCE can still maintain 86% of the control device (Table S1), which is similar to our previous study,[39] where PM6:Y6-based devices with relatively low content of PM6 still exhibited good device performance. However, when the AC174 content exceeds 50%, the PM6 content is too low, restricting the device performance. Because AC174 exhibits poor miscibility with PM6 or Y6, sufficient D:A interpenetrating networks are damaged, which decreases device performance. The statistic PCE distribution of optimized PM6:Y6 or PM6:AC174:Y6 based OSC devices are shown in Fig. S7a (ESI†), exhibiting good device reproducibility in both OSC devices. We have also measured the heat stability and light stability of PM6:Y6 and PM6:AC174:Y6 based OSC devices. The heat stability tests were carried out at 85 °C under nitrogen atmosphere (Fig. S8a, ESI†), where PM6:Y6 and PM6:AC174:Y6 devices exhibit similar heat stability. The light stability tests were measured under continuous AM 1.5G illumination under nitrogen atmosphere (Fig. S8b, ESI†). PM6:Y6 binary device retains 79% of original

PCE, while PM6:AC174:Y6 device retains 87% after continuous illumination for 300 min. Clearly, the introduction of AC174 improves the device light stability.

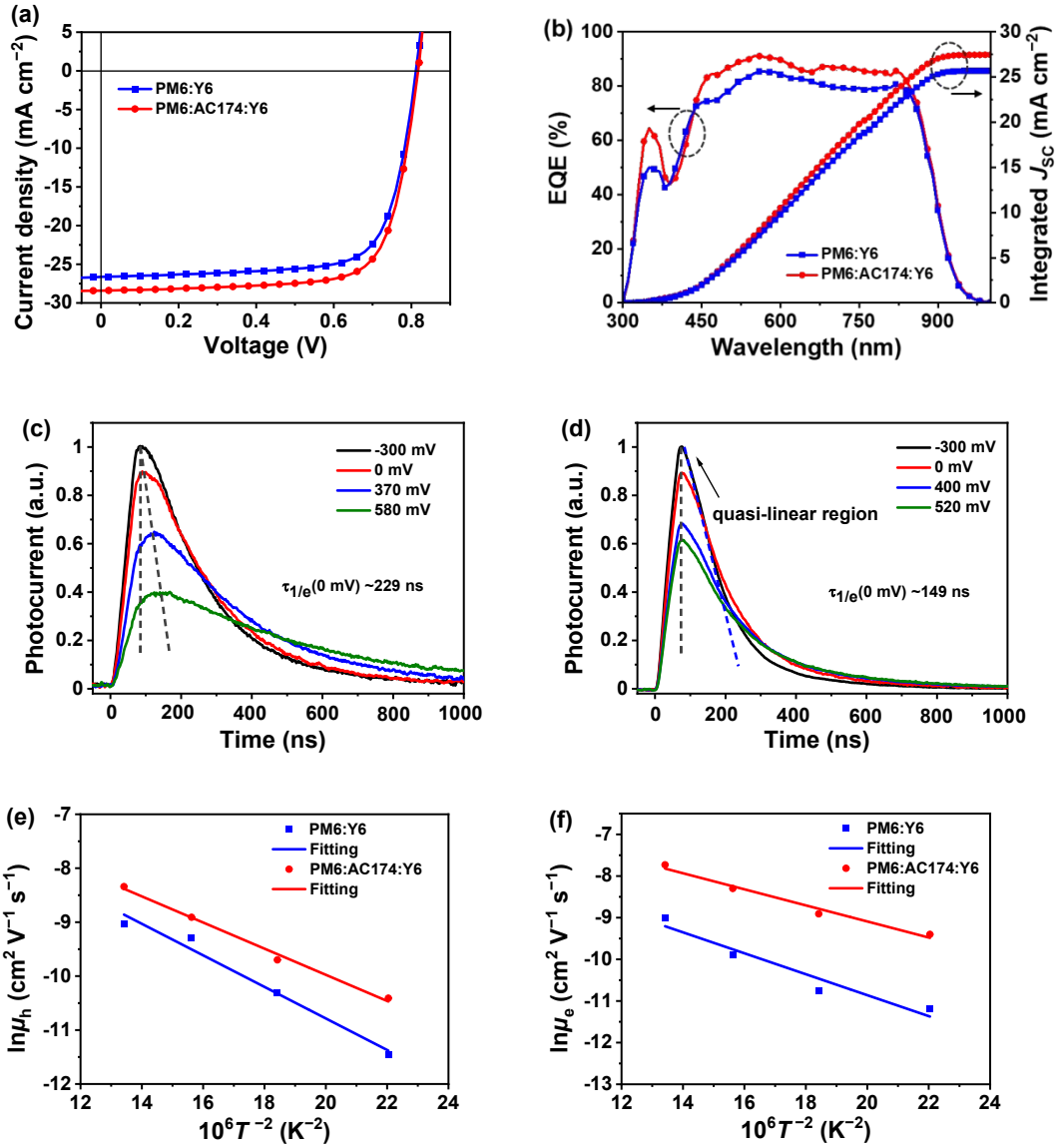

Fig. 2 (a) *J-V* curves and (b) EQE and integrated J_{SC} curves of optimized PM6:Y6 and PM6:AC174:Y6 devices. TPC curves of (c) PM6:Y6 and (d) PM6:AC174:Y6 devices under varied external bias voltage. Temperature dependence of hole mobility (e) and electron mobility (f) in PM6:Y6 and PM6:AC174:Y6 films in lnμ vs T^{-2} representation for quantitative analysis of the energy disorder.

Table 1 Performance of the optimized PM6:Y6 and PM6:AC174:Y6 based devices.[a]

Active layer	V_{OC} (V)	J_{SC} (mA cm^{-2})	FF (%)	PCE (%)	Calc. J_{SC} (mA cm^{-2})
PM6:Y6	0.812 (0.809±0.004)	26.6 (26.4±0.5)	73.5 (72.7±1.3)	15.9 (15.5±0.2)	26.0
PM6:AC174:Y6	0.817 (0.813±0.007)	28.4 (28.1±0.6)	74.1 (73.3±0.8)	17.2 (16.7±0.3)	27.9

[a] Average values (in parenthesis) are obtained from 10 devices.

The EQE spectra of optimized PM6:Y6 and PM6:AC174:Y6 devices are shown in Fig. 2b, where in the range of 450-800 nm, the EQE value of the ternary device is apparently higher than that of the device without AC174. The integrated J_{SC} values of PM6:Y6 and PM6:AC174:Y6 devices are 26.0 and 27.9 mA cm^{-2}, respectively, which agrees with the J_{SC} values measured from the *J-V* curves (less than 3% mismatch). Internal quantum efficiency (IQE) as a function of wavelength was also calculated, using the measured EQE and the active layer absorption determined by optical transfer matrix modelling simulations. As shown in Fig. S7b (ESI†), IQE was found to be higher for the device based on PM6:AC174:Y6, compared to that based on PM6:Y6, in the wavelength range of 580-680 nm. Since the optical property of the thin film of PM6:Y6 is hardly affected by the addition of AC174 (Fig. S9, ESI†), the higher IQE of the solar cell based on PM6:AC174:Y6 is most likely due to more efficient dissociation of excitons generated in the polymer donor, with an absorption peak at 620 nm.

To explore the origin of J_{SC} and IQE enhancement in the ternary device, modulated transient photocurrent (TPC) method was used to characterize the exciton dissociation of the devices.[40-41] We adopted a series of external bias voltages (from negative to positive) at the device to regulate the internal electric field. The TPC results of PM6:Y6 and PM6:AC174:Y6 devices are shown in Fig. 2c, 2d. TPC curves of both devices exhibit a fast rise and a relatively slow decay process. Nonetheless, difference in the dynamic characteristics between these two devices can be clearly seen. Firstly, on the condition of no external bias voltage (0 mV), the photocurrent of PM6:AC174:Y6 device takes 76 ns to reach the peak, which is 22 ns faster than that of PM6:Y6 device. At the same time, the ternary device exhibits a faster decay time of 149 ns, 80 ns faster than the device without AC174. The shortened photocurrent peak time and decay time of ternary device indicates a better exciton dissociation. Secondly, when weakening the internal electric field by applying a positive bias voltage, PM6:Y6 device needs longer time to reach photocurrent peak, while TPC peak time for PM6:AC174:Y6 device keeps unchanged at all voltages. These differences in the TPC results reflect difference in the exciton dissociation. PM6:Y6 device exhibits a relatively slow exciton dissociation, hence, it takes longer time to get photocurrent peak and decay at a low internal electric field because of dynamics equilibrium between exciton and free carriers.[42] For the ternary device, the improved exciton dissociation helps to weaken the dependence of the exciton dissociation dynamics on the internal electric field, thus making the TPC peak time unchanged at all the bias voltages. Thirdly, a quasi-linear region is observed in the TPC curve of PM6:AC174:Y6 device at an external bias voltage of −300 mV. This indicates that most of excitons in the

ternary device have been dissociated into free carriers to provide saturated charge concentration.[43] In contrast, such phenomenon is not observed in PM6:Y6 device, which implies that even under strong internal electric field, the exciton dissociation in the PM6:Y6 device is still insufficient. The TPC results reveal that the exciton dissociation in the PM6:AC174:Y6 device is more efficient than that in the device without AC174, which is responsible for the higher J_{SC} in ternary device.

The relationship between J_{SC} and light intensity (P_{light}) can be adopted to describe charge recombination (Fig. S10, ESI†). The J_{SC} follows a power-law relationship with P_{light} ($J_{SC} \propto P_{light}^{\alpha}$), where when α reaches 1, it means that all the charges have been collected by electrodes and no bimolecular recombination exists.[44] The α values of PM6:Y6 and PM6:AC174:Y6 devices are 0.939 and 0.946, respectively, indicating less bimolecular recombination in PM6:AC174:Y6 ternary device.

Charge mobility was measured to investigate the charge transport behaviour. We employed organic field-effect transistor (OFET) method to measure charge mobilities of PM6, AC174 and PM6:AC174 blend films in the horizontal direction (Fig. S11, ESI†). The hole mobilities (μ_h) of PM6, AC174 and PM6:AC174 blend films are 4.9×10^{-2} cm^2 V^{-1} s^{-1}, 3.5×10^{-3} cm^2 V^{-1} s^{-1} and 6.3×10^{-2} cm^2 V^{-1} s^{-1}, respectively. Compared with pristine PM6, the PM6:AC174 blend films exhibit a better charge transport in the horizontal direction. We next used space charge limited current (SCLC) method to measure charge mobilities of PM6:Y6, PM6:AC174:Y6 and AC174:Y6 blend films in the vertical direction (Fig. S12, Table S2, ESI†).[45] The μ_h of PM6:Y6, PM6:AC174:Y6, and AC174:Y6 blends are 9.1×10^{-4} cm^2 V^{-1}

s^{-1}, 1.1 × 10^{-3} cm^2 V^{-1} s^{-1}, and 6.1 × 10^{-4} cm^2 V^{-1} s^{-1}, respectively. The electron mobilities (μ_e) of above three blends are 8.3 × 10^{-4} cm^2 V^{-1} s^{-1}, 1.1 × 10^{-3} cm^2 V^{-1} s^{-1}, and 5.1 × 10^{-4} cm^2 V^{-1} s^{-1}, respectively. Compared with PM6:Y6 binary blend, the optimized ternary blend exhibits higher and more balanced charge mobilities, which can reduce charge recombination and improve FF.

Exciton and charge transport in amorphous or weak crystalline organic semiconductors is regarded as a hopping process between localized sites, following extended Gaussian disorder model (EGDM). The distribution of electronic density of states (DOS) in LUMO and HOMO energy levels follows a Gaussian curve (denoted as Δ_{HOMO} for HOMO energy level and Δ_{LUMO} for LUMO energy level) and the width of the Gaussian curve reflects the energy disorder of the material.[46,47] According to the EGDM, charge mobility is a function of temperature and material energy disorder at low electric fields, following the formula:

$$\mu(T) = c_1\mu_0 \exp\left(-c_2\left(\frac{\sigma}{k_B T}\right)^2\right) \quad (1)$$

where $\mu(T)$ is charge mobility, μ_0 is charge mobility with T approaching infinity, k_B is the Boltzmann constant, T is temperature, σ is the Gaussian width of DOS reflecting the energy disorder, c_1 and c_2 are constants, c_1 is 1.8 × 10^{-9} and c_2 is 0.42.[48-50] Temperature dependent charge mobility characterization was conducted for PM6:Y6 and PM6:AC174:Y6 blend films adopting SCLC method.

Here, we fabricated space-charge-limited hole-only devices with the structure of ITO/PEDOT:PSS/blend films/Au and electron-only devices with the structure of ITO/ZnO/blend films/BCP/Ag, and investigated the temperature-dependent charge mobility.

When the temperature decreases from 273 K to 213 K, the μ_h of PM6:Y6 binary device decreases from 1.2 × 10^{-4} cm^2 V^{-1} s^{-1} to 1.1 × 10^{-5} cm^2 V^{-1} s^{-1}, and that of PM6:AC174:Y6 ternary device decreases from 2.4 × 10^{-4} cm^2 V^{-1} s^{-1} to 3.0 × 10^{-5} cm^{-2} V^{-1} s^{-1} (Fig. S13a, S13b, ESI†); the μ_e of PM6:Y6 binary device decreases from 1.3 × 10^{-4} cm^2 V^{-1} s^{-1} to 1.4 × 10^{-5} cm^2 V^{-1} s^{-1}, while that of PM6:AC174:Y6 ternary device decreases from 4.4 × 10^{-4} cm^2 V^{-1} s^{-1} to 8.3 × 10^{-5} cm^{-2} V^{-1} s^{-1} (Fig. S13c, S13d, ESI†). We calculated the σ values of PM6:Y6 and PM6:AC174:Y6 blends alongside the Δ_{HOMO} and Δ_{LUMO} using Equation 1 (Fig. 2e, 2f). Regarding the energy disorder in the HOMO energy levels (σ_{HOMO}), PM6:AC174:Y6 blend film exhibits a smaller σ value of 107.7 meV compared with PM6:Y6 blend film (115.1 meV). Furthermore, a lower σ in the LUMO energy levels (σ_{LUMO}) was found for PM6:AC174:Y6 blend film (93.5 meV) compared with that of PM6:Y6 blend film (106.8 meV). The reduction in σ values along with increased charge mobility is beneficial for exciton diffusion/ dissociation and charge transport.

Device photophysics

The steady-state photoluminescence (PL) and transient gating ultrafast photoluminescence (TG-UFPL) were applied to investigate exciton diffusion and exciton dissociation in different films. As shown in Fig. 1c, AC174 film exhibits a strong PL emission in the range of 550-700 nm, with a relatively high PL quantum yield (PLQY) of 11.4%. The emission range of AC174 is highly overlapped with the absorption range of PM6, supporting the Förster energy transfer between AC174 and PM6. The PL spectra of pure PM6 and

PM6:AC174 (5%) blend films were measured under excitation at 600 nm (Fig. S14, ESI†). Neat AC174 and PM6 films exhibit emission peaks at 580 nm and 673 nm, respectively, while PM6:AC174 (5%) blend film exhibits an emission peak also at 673 nm, with stronger intensity and higher PLQY (2.85%) compared with PM6 (2.16%), indicating efficient energy transfer from AC174 to PM6. Compared with pure PM6, stronger PL intensity of PM6:AC174 blend is favourable for enhancing the long-range FRET between donor and acceptor and therefore exciton diffusion length.

To investigate the photo-excitation dynamics in more details, we applied TG-UFPL and transient absorption spectroscopy (TAS). The experimental details of these methods are included in the Supporting Information. Firstly, we used TG-UFPL to selectively probe the singlet exciton behaviour of PM6 donor in sub-picosecond to tens of picosecond, the critical time scale for the dissociation of PM6 excitons in PM6:Y6 blends.[51] Fig. 3a shows the PL emission of pure PM6 and PM6:AC174 blend films at a pump fluence of 2.44 μJ cm^{-2} with an excitation wavelength of 515 nm. We observed that PM6:AC174 blend has a longer emission decay of *ca.* 550 fs (amplitude weighted half-intensity) and pure PM6 has a shorter decay of *ca.* 400 fs, indicating a longer exciton lifetime in donor blend. The TG-UFPL's ultrashort gate time window (<200 fs) is only sensitive to singlet excitons, which have a high emissive rate, and not to late generated excimers.[51] The observed fast PL decays are consistent with the kinetics of Frenkel-type local excitation in PM6 measured by TAS,[51] suggesting that we are probing the key excitation species on critical time scale for photocurrent generation.

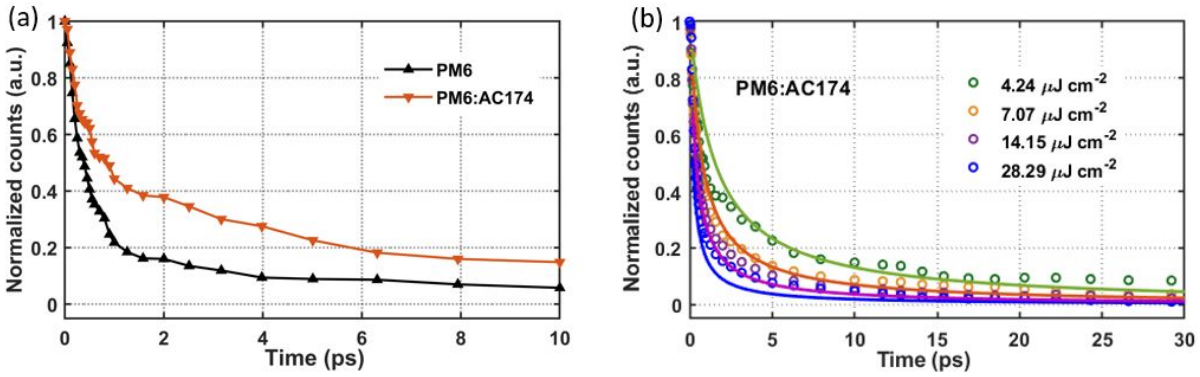

Fig. 3 (a) Integrated photoluminescence emission kinetics of PM6 and PM6:AC174 (5%) films. (b) global fitting of fluence dependent decays for PM6:AC174 (5%) films.

Then, we compared the fluence-dependent PL emission kinetics of pure PM6 film and PM6:AC174 (5%) blend film with a pump fluence ranging from 4.24 μJ cm^{-2} to 28.29 μJ cm^{-2} (Fig. S15, 3b, ESI†**)**. It can be seen that pure PM6 has no clear fluence dependence in the range of our experimental conditions, while the PM6:AC174 blend does. The lack of fluence dependence in PM6, which is consistent with previous transient experimental measurement under similar excitation densities,[31] indicates that the excitons aren't very mobile on this timescale. However, for the PM6:AC174 blend, exciton annihilation becomes stronger with increasing the excitation intensity, which indicates exciton diffusion ability considerably increases.

Furthermore, the bimolecular exciton recombination (exciton annihilation) decay rate (δ) can be determined according to the following Equation 2,

$$n(t) = \frac{n_i(0)e^{-kt}}{1+\frac{\delta}{2k}n_i(0)[1-e^{-kt}]} \quad (2)$$

where $n(t)$ is the experimental excitation density (excitations cm^{-3}), t is the time, $n_i(0)$ is the initial excitation density for each fluence (excitations cm^{-3}), and k is the monomolecular decay constant[30] (for PM6, $k = 1.83 \times 10^9$ s^{-1}). We fitted the experimental fluence dependent decays to get the bimolecular exciton recombination decay rate δ (cm^3 s^{-1}). Since we didn't observe intensity dependent PL kinetics of the PM6 films, we fitted the PL kinetics with Eq. 2 to obtain δ values for each fluence dependent decays. On the other hand, for PM6:AC174, we employed global fitting to extract single δ value from the fluence dependent decays. Fitting parameters are detailed in Table S3 (ESI†**)**. The bimolecular exciton recombination decay rate (δ) of PM6:AC174 blend is calculated to be 1.44×10^{-6} cm^3 s^{-1}, which is higher than the highest value, 6.39×10^{-7} cm^3 s^{-1}, obtained from pure PM6. In polymer solar cells, a general feature is ultrafast (<10 ps) photocurrent generation when the donor polymers are excited, and this behaviour requires efficient exciton transport for exciton to reach the donor/acceptor interface within its lifetime. Based on the δ values, we can estimate exciton diffusion constant (D) by $\delta/(8\pi r)$, where r is the annihilation radius approximated as 1 nm[30] and the exciton diffusion length L_D at time τ after the photoexcitation by $\sqrt{D\tau}$. After calculation, PM6:AC174 blend exhibits a higher D value (0.573 cm^2 s^{-1}) and a longer L_D value within the relevant charge generation timescale of 10 ps (25 nm) compared with pure PM6 (0.239 cm^2 s^{-1}, 15 nm), which indicates a better ability to facilitate rapid exciton diffusion cross PM6 domain in PM6:AC174 blend.

The longer exciton diffusion length is beneficial for exciton dissociation in D/A blend systems. We compared the ultrafast PL emission of pure PM6, PM6:Y6 binary blend and

PM6:AC174:Y6 ternary blend films at a pump fluence of 7.07 μJ cm^{-2} (Fig. S16, ESI†). Although 515 nm excitation excites both PM6 and Y6 in the blend thin films, our ultrafast PL, which cannot detect the emission from Y6 due to the sensitivity of the camera, selectively probe PM6 singlet exciton dynamics to avoid the complicated data interpretations involving multiple excitation species. We can estimate the exciton quenching efficiency by comparing the exciton decay time of the donor in the presence and absence of the acceptor. As shown in Fig. S16 (ESI†), the PM6 singlet excitons in PM6:Y6 binary and PM6:AC174:Y6 ternary blends have similar decay times (*ca.* 300 fs); however, considering PM6 exciton in PM6:AC174 has a longer decay time than the pure PM6 (550 fs versus 400 fs), we can conclude that the exciton quenching is more efficient in the ternary blends, indicating a faster D/A energy transfer[31] and exciton diffusion accompanying with better exciton dissociation and charge generation.

We next employ TAS measurement to observe the charge dynamics when the Y6 molecules are excited. Measurements were conducted with an 800 nm excitation wavelength to selectively excite Y6 with pump fluences ranging from 5 μW to 20 μW. Fig. S17 (ESI†) shows the TAS spectra of the binary and ternary blends with a pump fluence of 20 μW. The photo induced absorption (PIA) band is shown as a negative feature around 955 nm. Two positive peaks are observed around 860 nm and 610 nm which can be assigned as an overlapping contribution of the Y6 bleach signal and PM6 bleach signal. The positive ground state bleaching (GSB) signal in the 575-625 nm region of the PM6 gauges the charge generation process. Since PM6 is not excited at 800 nm, PM6 bleaching comes about when

photoexcitation in Y6 undergo hole transfer to PM6.[52] Therefore, PM6 bleaching is proportional to the total charge population. As shown in Fig. 4, the charge formation kinetics shows no distinct difference between the binary and ternary thin films, indicating similar charge formation/exciton dissociation dynamics. However, after the charge formation reaches to peak, when the pump-probe delay time is about 50 ps, it can be seen that the PM6:AC174:Y6 ternary blend has a more pronounced non-geminate charge recombination at high excitation density (substantially higher than encountered under solar excitation conditions). This, in turn, suggests more efficient generation of more mobile charges in the ternary blend, in accordance with SCLC results. Overall, the PM6:AC174:Y6 ternary OSC exhibits a longer exciton diffusion length, a better exciton dissociation ability and a better charge transport ability. This is likely owing to its lower system energetic disorder, benefitting from its better nanostructure morphology, which is studied in the following section.

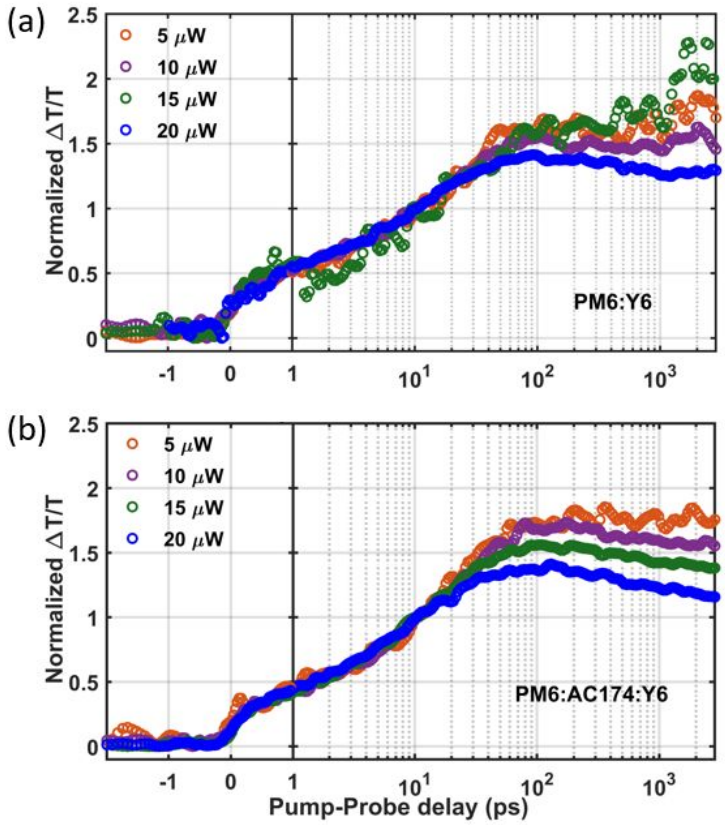

Fig. 4 Fluence dependent kinetics of the GSB signal for (a) PM6:Y6 and (b) PM6:AC174:Y6 films under an 800 nm excitation pump, intensity normalized at 10 ps.

Film morphology

The contact angle measurements were used to study the surface tension of materials and evaluate the miscibility between materials. The surface tensions of materials were calculated from measured contact angles on water and diiodomethane using the Owens–Wendt equation.[53] The results are shown in Table S4 and Fig. S18 (ESI†**)**. The Flory-Huggins interaction parameters (χ) were calculated applying the equation of $\chi = (\sqrt{\gamma_A} - \sqrt{\gamma_B})^2$.[54] According to the Flory-Huggins model, a smaller χ indicates stronger interaction between two components, namely, better miscibility. The interaction parameter between PM6 and Y6 is

relatively low ($\chi_{PM6:Y6}$ = 0.045), indicating a remarkable miscibility between them. The interaction parameter between PM6:AC174 (5%) blend donors and Y6 is 0.095, which is a little larger than that of the PM6:Y6 system. On one hand, a pretty good miscibility still exists between blend donors and acceptor. On the other hand, slightly decreased D/A miscibility is beneficial for Y6 molecular packing, which is favourable for decreasing energetic disorder and improving exciton diffusion/dissociation and charge transport. In contrast, the χ values between AC174 and PM6 or Y6 are considerably larger ($\chi_{AC174:PM6}$ = 0.442; $\chi_{AC174:Y6}$ = 0.770), indicating that AC174 has a poor miscibility with PM6 or Y6.

Transmission electron microscopy (TEM) was employed to study the film morphology of PM6:Y6, PM6:AC174:Y6, AC174:Y6 and PM6:AC174 blend films (Fig. S19, ESI†). PM6:Y6 and PM6:AC174:Y6 films exhibit smooth morphology. AC174:Y6 blend film exhibits large phase domain size, which can be attributed to the poor miscibility between AC174 and Y6. As for the PM6:AC174 film, because we added a small amount of AC174 (5%), the phase separation cannot be clearly seen. Furthermore, we used atomic force microscopy (AFM) to investigate the surface morphology of PM6:Y6, PM6:AC174:Y6, and AC174:Y6 blend films (Fig. S20, ESI†). The root-mean-square roughness (R_q) of PM6:Y6, PM6:AC174:Y6, and AC174:Y6 blend films are 1.22 nm, 1.23 nm, and 6.61 nm, respectively. AC174:Y6 blend film exhibits rough surface morphology, owing to poor miscibility between them.

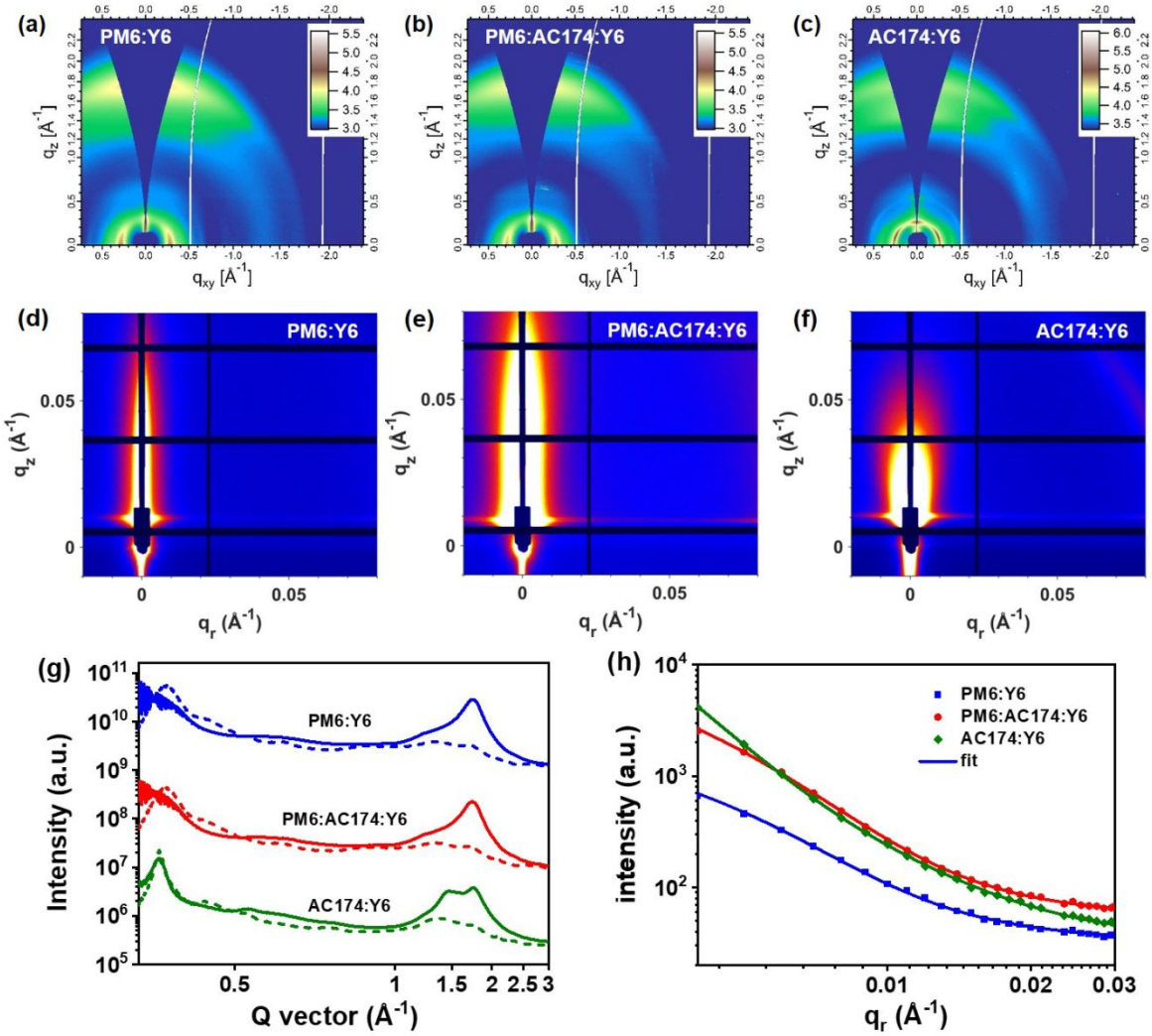

Fig. 5 (a-c) 2D GIWAXS patterns and (d-f) 2D GISAXS patterns of PM6:Y6, PM6:AC174:Y6, and AC174:Y6 thin films, respectively. (g) Corresponding GIWAXS profiles in the out-of-plane (solid lines) and in-plane (dashed lines) directions. (h) Corresponding GISAXS fitted scattering intensity along the in-plane direction.

GIWAXS characterizations were performed to evaluate molecular packing and orientation of pure and blend films.[55,56] The two-dimensional GIWAXS (2D-GIWAXS) patterns and corresponding 1D line-cuts along the in-plane and out-of-plane directions of pure films and PM6:AC174 blend films are shown in Fig. S21 (ESI†) and Fig. 1b. The pure Y6

film exhibits high crystallinity with a preferential face-on orientation indicated by the π–π peak along the q_z axis (q = 1.74 Å^{-1}, d = 3.62 Å). The pure PM6 film was reported to be preferentially face-on oriented with the π–π peak at q_z= 1.69 Å^{-1} (d = 3.72 Å), and the coherence length (CL) is 1.86 nm. The PM6:AC174 (5%) blend film exhibits the π–π peak along the q_z axis (q_z= 1.69 Å^{-1}, d = 3.72 Å), and the CL increases to 1.99 nm. A stronger π–π stacking of PM6 along the q_z axis is beneficial for decreasing energetic disorder and improving charge transport in the vertical direction.

The 2D-GIWAXS patterns and corresponding 1D line-cuts along the in-plane and out-of-plane directions of PM6:Y6, PM6:AC174:Y6 and AC174:Y6 blend films are shown in Fig. 5a-c, 5g. For the AC174:Y6 blend film, π–π peaks located at q_z = 1.49 Å^{-1} and q_z = 1.75 Å^{-1} are attributed to the scattering from face-on oriented AC174 and Y6 crystalline domains, respectively, without forming co-crystal structure, which indicates poor miscibility between the two materials. For PM6:Y6 and PM6:AC174:Y6 blend films, π–π peaks locate at q_z = 1.75 Å^{-1} (d = 3.60 Å) and q_z = 1.74 Å^{-1} (d = 3.61 Å), respectively, and the corresponding CL values slightly increase from 2.86 nm to 2.87 nm. Both blend films exhibit evident Y6 ordering in the out-of-plane direction, leading to good charge transport.

Grazing incidence small-angle X-ray scattering (GISAXS) measurements were conducted to characterize phase separation of the binary and ternary blends (Fig. 5d-f, 5h).[57] The Debye-Anderson-Brumberger (DAB) model and the fractal-like network model were used to evaluate the intermixing amorphous phases and pure acceptor domains, respectively, in GISAXS measurements.[58] The correlation lengths of the intermixing region (ξ) of PM6:Y6,

PM6:AC174:Y6, and AC174:Y6 blend films are 21.2 nm, 25.4 nm, and 50.5 nm, respectively. The corresponding pure acceptor ($2R_g$) domain sizes are fitted to be 13.2 nm, 34.2 nm, and 46.8 nm, respectively. The domain size of pure acceptor region for AC174:Y6 much larger compared with PM6:Y6 and PM6:AC174:Y6, which is consistent with the poor miscibility between AC174:Y6. Compared with PM6:Y6 blend, the relatively larger intermixing region length of ternary blend film may contribute to exciton dissociation in this region, consistent with the TPC and TG-UFPL results, leading to higher J_{SC} values in devices. The great increase of pure acceptor domain sizes in the ternary blend film is related to the higher crystallinity of Y6, which facilitates charge transport, confirmed by the SCLC measurements. Moreover, increased Y6 domain size is beneficial for reducing system energetic disorder, leading to longer exciton diffusion length, consistent with the TG-UFPL data.

Conclusions

In summary, a highly crystalline, highly emissive, and wide-bandgap polymer AC174 with an extremely small Stokes shift was synthesized in water and was added into the PM6:Y6 blend to fabricate PM6:AC174:Y6 ternary OSC devices. AC174 exhibits poor compatibility with PM6 and Y6, which tends to form an individual phase in ternary films, improves the molecular packing, and reduces system energetic disorder, which is beneficial for FRET and exciton transport. The heavily overlapping of AC174 absorption and PM6 emission spectra as well as high PLQY of AC174 facilitate FRET between AC174 and PM6, leading to better exciton diffusion ability, longer exciton lifetime and longer exciton diffusion

length in PM6:AC174 blend. Relative to the PM6:Y6 binary devices, the PM6:AC174:Y6 ternary OSCs exhibit a longer exciton diffusion length, more efficient exciton dissociation, charge generation and charge transport. As a result, the ternary OSCs based on PM6:AC174:Y6 yield a PCE of 17.2%, which is higher than that of the PM6:Y6 binary devices (15.9%). It is worth noting that the ternary devices exhibit the highest IQE approaching 100% and an impressive J_{SC} value over 28 mA cm^{-2}. This study provides a facile strategy of morphology optimization, reducing system energetic disorder, enhancing exciton diffusion length by introducing a polymer semiconductor with high crystallinity, high PLQY, and small Stokes shift, and finally improving the performance of the OSCs.

Acknowledgements

X.Z. thanks the NSFC (Nos. U21A20101 and 21734001). W.M. thanks the NSFC (21704082, 21875182), Key Scientific and Technological Innovation Team Project of Shaanxi Province (2020TD-002), 111 Project 2.0 (BP2018008). GIWAXS data was acquired at beamlines 7.3.3 at the Advanced Light Source, which is supported by the Director, Office of Science, Office of Basic Energy Sciences, of the U.S. Department of Energy under Contract No. DE-AC02-05CH11231. The authors thank Dr. Eric Schaible and Dr. Chenhui Zhu at beamline 7.3.3 for assistance with data acquisition.

Conflict of Interest

The authors declare no conflict of interest.

Notes and references

1. L. Lu, T. Zheng, Q. Wu, A. M. Schneider, D. Zhao and L. Yu, *Chem. Rev.*, 2015, **115**, 12666-12731.

2. C. Yan, S. Barlow, Z. Wang, H. Yan, A. K. Y. Jen, S. R. Marder and X. Zhan, *Nat. Rev. Mater.*, 2018, **3**, 18003.

3. J. Wang, P. Xue, Y. Jiang, Y. Huo and X. Zhan, *Nat. Rev. Chem.*, 2022, **6**, 614-634.

4. J. Wang and X. Zhan, *Acc. Chem. Res.*, 2021, **54**, 132-143.

5. Y. Lin, J. Wang, Z.-G. Zhang, H. Bai, Y. Li, D. Zhu and X. Zhan, *Adv. Mater.*, 2015, **27**, 1170-1174.

6. Y. Lin, Q. He, F. Zhao, L. Huo, J. Mai, X. Lu, C.-J. Su, T. Li, J. Wang, J. Zhu, Y. Sun, C. Wang and X. Zhan, *J. Am. Chem. Soc.*, 2016, **138**, 2973-2976.

7. Y. Lin, F. Zhao, Q. He, L. Huo, Y. Wu, T. C. Parker, W. Ma, Y. Sun, C. Wang, D. Zhu, A. J. Heeger, S. R. Marder and X. Zhan, *J. Am. Chem. Soc.*, 2016, **138**, 4955-4961.

8. S. Dai, F. Zhao, Q. Zhang, T.-K. Lau, T. Li, K. Liu, Q. Ling, C. Wang, X. Lu, W. You and X. Zhan, *J. Am. Chem. Soc.*, 2017, **139**, 1336-1343.

9. J. Wang, J. Zhang, Y. Xiao, T. Xiao, R. Zhu, C. Yan, Y. Fu, G. Lu, X. Lu, S. R. Marder and X. Zhan, *J. Am. Chem. Soc.*, 2018, **140**, 9140-9147.

10. J. Yuan, Y. Zhang, L. Zhou, G. Zhang, H.-L. Yip, T.-K. Lau, X. Lu, C. Zhu, H. Peng, P. A. Johnson, M. Leclerc, Y. Cao, J. Ulanski, Y. Li and Y. Zou, *Joule*, 2019, **3**, 1140-1151.

11. Y. Ma, M. Zhang, S. Wan, P. Yin, P. Wang, D. Cai, F. Liu and Q. Zheng, *Joule*, 2021, **5**, 197-209.

12. C. Li, J. Zhou, J. Song, J. Xu, H. Zhang, X. Zhang, J. Guo, L. Zhu, D. Wei, G. Han, J. Min, Y. Zhang, Z. Xie, Y. Yi, H. Yan, F. Gao, F. Liu and Y. Sun, *Nat. Energy*, 2021, **6**, 605-613.

13. L. Zhu, M. Zhang, J. Xu, C. Li, J. Yan, G. Zhou, W. Zhong, T. Hao, J. Song, X. Xue, Z. Zhou, R. Zeng, H. Zhu, C.-C. Chen, R. C. I. MacKenzie, Y. Zou, J. Nelson, Y. Zhang, Y. Sun and F. Liu, *Nat. Mater.*, 2022, **21**, 656-663.

14. K. Chong, X. Xu, H. Meng, J. Xue, L. Yu, W. Ma and Q. Peng, *Adv. Mater.*, 2022, **34**, 2109516.

15. Z. Zheng, J. Wang, P. Bi, J. Ren, Y. Wang, Y. Yang, X. Liu, S. Zhang and J. Hou, *Joule*, 2022, **6**, 171-184.

16. O. G. Reid, R. D. Pensack, Y. Song, G. D. Scholes and G. Rumbles, *Chem. Mater.*, 2014, **26**, 561-575.

17. R. A. J. Janssen and J. Nelson, *Adv. Mater.*, 2013, **25**, 1847-1858.

18. O. V. Mikhnenko, P. W. M. Blom and T.-Q. Nguyen, *Energy Environ. Sci.*, 2015, **8**, 1867-1888.

19. Y. Tamai, H. Ohkita, H. Benten and S. Ito, *J. Phys. Chem. Lett.*, 2015, **6**, 3417-3428.

20. Z. Zhou, S. Xu, J. Song, Y. Jin, Q. Yue, Y. Qian, F. Liu, F. Zhang and X. Zhu, *Nat. Energy*, 2018, **3**, 952-959.

21. L. Ye, H. Hu, M. Ghasemi, T. Wang, B. A. Collins, J.-H. Kim, K. Jiang, J. H. Carpenter, H. Li, Z. Li, T. McAfee, J. Zhao, X. Chen, J. L. Y. Lai, T. Ma, J.-L. Bredas, H. Yan and H. Ade, *Nat. Mater.*, 2018, **17**, 253-260.

22. J. Du, K. Hu, J. Zhang, L. Meng, J. Yue, I. Angunawela, H. Yan, S. Qin, X. Kong, Z. Zhang, B. Guan, H. Ade and Y. Li, *Nat. Commun.*, 2021, **12**, 5264.

23. T. Liu, T. Yang, R. Ma, L. Zhan, Z. Luo, G. Zhang, Y. Li, K. Gao, Y. Xiao, J. Yu, X. Zou, H. Sun, M. Zhang, T. A. D. Peña, Z. Xing, H. Liu, X. Li, G. Li, J. Huang, C. Duan, K. S. Wong, X. Lu, X. Guo, F. Gao, H. Chen, F. Huang, Y. Li, Y. Li, Y. Cao, B. Tang and H. Yan, *Joule*, 2021, **5**, 914-930.

24. M. Theander, A. Yartsev, D. Zigmantas, V. Sundström, W. Mammo, M. R. Andersson and O. Inganäs, *Phys. Rev. B*, 2000, **61**, 12957.

25. S. M. Menke and R. J. Holmes, *Energy Environ. Sci.*, 2014, **7**, 499-512.

26. R. Englman and J. Jortner, *Mol. Phys.*, 1970, **18**, 145-164.

27. S. D. Dimitrov, B. C. Schroeder, C. B. Nielsen, H. Bronstein, Z. Fei, I. McCulloch, M. Heeney and J. R. Durrant, *Polymers*, 2016, **8**, 14.

28. S. Karuthedath, J. Gorenflot, Y. Firdaus, N. Chaturvedi, C. S. P. D. Castro, G. T. Harrison, J. I. Khan, A. Markina, A. H. Balawi, T. A. D. Peña, W. Liu, R.-Z. Liang, A. Sharma, S. H. K. Paleti, W. Zhang, Y. Lin, E. Alarousu, S. Lopatin, D. H. Anjum, P.

M. Beaujuge, S. D. Wolf, I. McCulloch, T. D. Anthopoulos, D. Baran, D. Andrienko and F. Laquai, *Nat. Mater.*, 2021, **20**, 378-384.

29. P. Cheng, G. Li, X. Zhan and Y. Yang, *Nat. Photon.*, 2018, **12**, 131-142.

30. S. Chandrabose, K. Chen, A. J. Barker, J. J. Sutton, S. K. K. Prasad, J. Zhu, J. Zhou, K. C. Gordon, Z. Xie, X. Zhan and J. M. Hodgkiss, *J. Am. Chem. Soc.*, 2019, **141**, 6922-6929.

31. S. Y. Park, S. Chandrabose, M. B. Price, H. S. Ryu, T. H. Lee, Y. S. Shin, Z. Wu, W. Lee, K. Chen, S. Dai, J. Zhu, P. Xue, X. Zhan, H. Y. Woo, J. Y. Kim and J. M. Hodgkiss, *Nano Energy*, 2021, **84**, 105924.

32. S. Xie, Y. Xia, Z. Zheng, X. Zhang, J. Yuan, H. Zhou and Y. Zhang, *Adv. Funct. Mater.*, 2018, **28**, 1705659.

33. Z. Zhang, Y. Li, G. Cai, Y. Zhang, X. Lu and Y. Lin, *J. Am. Chem. Soc.*, 2020, **142**, 18741-18745.

34. S. Liu, J. Yuan, W. Deng, M. Luo, Y. Xie, Q. Liang, Y. Zou, Z. He, H. Wu and Y. Cao, *Nat. Photon.*, 2020, **14**, 300-305.

35. W. Deng, W. Liu, R. Qian and H. Wu, *J. Phys. Chem. Lett.*, 2022, **13**, 544-551.

36. A. Sanzone, A. Calascibetta, M. Monti, S. Mattiello, M. Sassi, F. Corsini, G. Griffini, M. Sommer and L. Beverina, *ACS Macro Lett.*, 2020, **9**, 1167-1171.

37. C. Li, X. Zhang, N. Yu, X. Gu, L. Qin, Y. Wei, X. Liu, J. Zhang, Z. Wei, Z. Tang, Q. Shi and H. Huang, *Adv. Funct. Mater.*, 2022, **32**, 2108861.

38. T. Li, K. Wang, G. Cai, Y. Li, H. Liu, Y. Jia, Z. Zhang, X. Lu, Y. Yang and Y. Lin, *JACS Au*, 2021, **1**, 1733-1742.

39. Y. Wang, M. B. Price, R. S. Bobba, H. Lu, J. Xue, Y. Wang, M. Li, A. Ilina, P. A. Hume, B. Jia, T. Li, Y. Zhang, N. J. L. K. Davis, Z. Tang, W. Ma, Q. Qiao, J. M. Hodgkiss and X. Zhan, *Adv. Mater.*, 2022, DOI: 10.1002/adma.202206717.

40. J. Shi, D. Li, Y. Luo, H. Wu and Q. Meng, *Rev. Sci. Instrum.*, 2016, **87**, 123107.

41. Y. Li, J. Shi, B. Yu, B. Duan, J. Wu, H. Li, D. Li, Y. Luo, H. Wu and Q. Meng, *Joule*, 2020, **4**, 472-489.

42. X. Zhao, B. Mi, Z. Gao and W. Huang, *Sci. China Phys. Mech. Astron.*, 2011, **54**, 375-387.

43. J. Seifter, Y. Sun and A. J. Heeger, *Adv. Mater.*, 2014, **26**, 2486-2493.

44. P. Schilinsky, C. Waldauf and C. J. Brabec, *Appl. Phys. Lett.*, 2002, **81**, 3885-3887.

45. G. G. Malliaras, J. R. Salem, P. J. Brock and C. Scott, *Phys. Rev. B*, 1998, **58**, 13411-13414.

46. C. Tanase, E. J. Meijer, P. W. M. Blom and D. M. de Leeuw, *Phys. Rev. Lett.*, 2003, **91**, 216601.

47. D. Abbaszadeh, A. Kunz, G. A. H. Wetzelaer, J. J. Michels, N. I. Crăciun, K. Koynov, I. Lieberwirth and P. W. M. Blom, *Nat. Mater.*, 2016, **15**, 628-633.

48. H. Bässler, *Phys. Status Solidi B*, 1993, **175**, 15-56.

49. W. F. Pasveer, J. Cottaar, C. Tanase, R. Coehoorn, P. A. Bobbert, P. W. M. Blom, D. M. de Leeuw and M. A. J. Michels, *Phys. Rev. Lett.*, 2005, **94**, 206601.

50. Y. Jiang, J. Wang, H. Zai, D. Ni, J. Wang, P. Xue, N. Li, B. Jia, H. Lu, Y. Zhang, F. Wang, Z. Guo, Z. Bi, H. Xie, Q. Wang, W. Ma, Y. Tu, H. Zhou and X. Zhan, *J. Am. Chem. Soc.*, 2022, **144**, 5400-5410.

51. R. Wang, C. Zhang, Q. Li, Z. Zhang, X. Wang and M. Xiao, *J. Am. Chem. Soc.*, 2020, **142**, 12751-12759.

52. M. B. Price, P. A. Hume, A. Ilina, I. Wagner, R. R. Tamming, K. E. Thorn, W. Jiao, A. Goldingay, P. J. Conaghan, G. Lakhwani, N. J. L. K. Davis, Y. Wang, P. Xue, H. Lu, K. Chen, X. Zhan and J. M. Hodgkiss, *Nat. Commun.*, 2022, **13**, 2827.

53. D. K. Owens and R. C. Wendt, *J. Appl. Polym. Sci.*, 1969, 13, 1741-1747.

54. S. Nilsson, A. Bernasik, A. Budkowski and E. Moons, *Macromolecules*, 2007, **40**, 8291-8301.

55. F. Liu, Y. Gu, X. Shen, S. Ferdous, H.-W. Wang and T. P. Russell, *Prog. Polym. Sci.*, 2013, **38**, 1990-2052.

56. J. Mai, Y. Xiao, G. Zhou, J. Wang, J. Zhu, N. Zhao, X. Zhan and X. Lu, *Adv. Mater.*, 2018, **30**, 1802888.

57. J. Mai, T.-K. Lau, J. Li, S.-H. Peng, C.-S. Hsu, U.-S. Jeng, J. Zeng, N. Zhao, X. Xiao and X. Lu, *Chem. Mater.*, 2016, **28**, 6186-6195.

58. J. Mai, H. Lu, T.-K. Lau, S.-H. Peng, C.-S. Hsu, W. Hua, N. Zhao, X. Xiao and X. Lu, *J. Mater. Chem. A*, 2017, **5**, 11739-11745.